Title

HD 202772A b: A Transiting Hot Jupiter around a Bright, Mildly Evolved Star in a Visual Binary Discovered by TESS

Journal

The Astronomical Journal, 157(2)

ISSN

0004-6256

Authors

Wang, Songhu
Jones, Matias
Shporer, Avi
et al.

Publication Date

2019-02-01

DOI

10.3847/1538-3881/aaf1b7

Peer reviewed

Draft version October 5, 2018
Typeset using LaTeX **twocolumn** style in AASTeX61

HD 202772A b: A TRANSITING HOT JUPITER AROUND A BRIGHT, MILDLY EVOLVED STAR IN A VISUAL BINARY DISCOVERED BY *TESS*

Songhu Wang,[1,2] Matias Jones,[3] Avi Shporer,[4] Benjamin J. Fulton,[5,6] Leonardo A. Paredes,[7] Trifon Trifonov,[8] Diana Kossakowski,[8] Jason Eastman,[9] Maximilian N. Günther,[4,10] Chelsea X. Huang,[4,10] Sarah Millholland,[1,11] Darryl Seligman,[1] Debra Fischer,[1] Rafael Brahm,[12,13,14] Xian-Yu Wang,[15,16] Bryndis Cruz,[1] Hodari-Sadiki James,[7] Brett Addison,[17] Todd Henry,[18] En-Si Liang,[19] Allen B. Davis,[1] René Tronsgaard,[20] Keduse Worku,[1] John Brewer,[1] Martin Kürster,[8] Charles A. Beichman,[6] Allyson Bieryla,[9] Timothy M. Brown,[21,22] Jessie L. Christiansen,[6] David R. Ciardi,[6] Karen A. Collins,[9] Gilbert A. Esquerdo,[9] Andrew W. Howard,[5] Howard Isaacson,[23] David W. Latham,[9] Tsevi Mazeh,[24] Erik A. Petigura,[5] Samuel N. Quinn,[9] Sahar Shahaf,[24] Robert J. Siverd,[25] George R. Ricker,[4] Roland Vanderspek,[4] Sara Seager,[4,26] Joshua N. Winn,[27] Jon M. Jenkins,[28] Patricia T. Boyd,[29] Gábor Fűrész,[4] Christopher Henze,[28] Alen M. Levine,[4] Robert Morris,[30] Martin Paegert,[9] Keivan G. Stassun,[25,31] Eric B. Ting,[28] Michael Vezie,[4] and Gregory Laughlin[1]

[1] *Department of Astronomy, Yale University, New Haven, CT 06511, USA*
[2] *51 Pegasi b Fellow*
[3] *European Southern Observatory, Casilla 19001, Santiago, Chile*
[4] *Department of Physics and Kavli Institute for Astrophysics and Space Research, Massachusetts Institute of Technology, Cambridge, MA 02139, USA*
[5] *California Institute of Technology, Pasadena, CA 91125, USA*
[6] *IPAC-NASA Exoplanet Science Institute Pasadena, CA 91125, USA*
[7] *Physics and Astronomy Department, Georgia State University, Atlanta, GA 30302, USA*
[8] *Max-Planck-Institut für Astronomie, Königstuhl 17, 69117 Heidelberg, Germany*
[9] *Harvard-Smithsonian Center for Astrophysics, 60 Garden Street, Cambridge, MA 02138, USA*
[10] *Juan Carlos Torres Fellow*
[11] *NSF Graduate Research Fellow*
[12] *Center of Astro-Engineering UC, Pontificia Universidad Católica de Chile, Av. Vicuña Mackenna 4860, 7820436 Macul, Santiago, Chile*
[13] *Instituto de Astrofísica, Pontificia Universidad Católica de Chile, Av. Vicuña Mackenna 4860, Macul, Santiago, Chile*
[14] *Millennium Institute for Astrophysics, Chile*
[15] *Key Laboratory of Optical Astronomy, National Astronomical Observatories, Chinese Academy of Sciences, Beijing 100012, China*
[16] *University of Chinese Academy of Sciences, Beijing, 100049, China*
[17] *University of Southern Queensland, Toowoomba, Qld 4350, Australia*
[18] *RECONS Institute, Chambersburg, PA, USA*
[19] *School of Astronomy and Space Science & Key Laboratory of Modern Astronomy and Astrophysics in Ministry of Education, Nanjing University, Nanjing 210023, China*
[20] *DTU Space, National Space Institute, Technical University of Denmark, Elektrovej 328, DK-2800 Kgs. Lyngby, Denmark*
[21] *Las Cumbres Observatory, 6740 Cortona Dr., Suite 102, Goleta, CA 93117, USA*
[22] *University of Colorado/CASA, Boulder, CO 80309, USA.*
[23] *Astronomy Department, University of California, Berkeley, CA 94720, USA*
[24] *School of Physics and Astronomy, Tel Aviv University, Tel Aviv 69978, Israel*
[25] *Department of Physics and Astronomy, Vanderbilt University, Nashville, TN 37235, USA*
[26] *Earth and Planetary Sciences, MIT, 77 Massachusetts Avenue, Cambridge, MA 02139, USA*
[27] *Department of Astrophysical Sciences, Princeton University, 4 Ivy Lane, Princeton, NJ 08544, USA*
[28] *NASA Ames Research Center, Moffett Field, CA 94035, USA*
[29] *NASA Goddard Space Flight Center, 8800 Greenbelt Road, Greenbelt, MD 20771, USA*

Corresponding author: Songhu Wang
song-hu.wang@yale.edu

[30] *SETI Institute*
[31] *Department of Physics, Fisk University, Nashville, TN 37208, USA*

ABSTRACT

We report the first confirmation of a hot Jupiter discovered by the *Transiting Exoplanet Survey Satellite* (*TESS*) mission: HD 202772A b. The transit signal was detected in the data from *TESS* Sector 1, and was confirmed to be of planetary origin through radial velocity (RV) measurements. HD 202772A b is orbiting a mildly evolved star with a period of 3.3 days. With an apparent magnitude of $V = 8.3$, the star is among the brightest known to host a hot Jupiter. Based on the 27 days of *TESS* photometry, and RV data from the CHIRON and HARPS spectrographs, the planet has a mass of $1.008^{+0.074}_{-0.079}\,M_J$ and radius of $1.562^{+0.053}_{-0.069}\,R_J$, making it an inflated gas giant. HD 202772A b is a rare example of a transiting hot Jupiter around a quickly evolving star. It is also one of the most strongly irradiated hot Jupiters currently known.

Keywords: planetary systems, planets and satellites: detection, stars: individual (TIC 290131778, TOI 123, HD 202772)

1. INTRODUCTION

Hot Jupiters, owing to their ease of detectability, are the best-studied population of extrasolar planets. However, we still do not understand how these behemoths came into existence. Did they form *in situ* (Bodenheimer et al. 2000; Batygin et al. 2016), or did they arise in wider orbits and migrate to their current locations (Lin et al. 1996)? If hot Jupiters did undergo migration, was this process violent (Wu et al. 2007; Rasio & Ford 1996; Wu & Lithwick 2011; Petrovich 2015) or quiescent (Lin et al. 1996)? Are the highly inclined and eccentric orbits of some hot Jupiters a consequence of high-eccentricity migration (Winn et al. 2010; Bonomo et al. 2017), or other mechanisms that are unrelated to planet migration (Lai 2016; Duffell & Chiang 2015)? What is the occurrence rate of hot Jupiters as a function of stellar age (Donati et al. 2016)? What is the meaning of the high rate of distant companions (Knutson et al. 2014) and the low rate of close-in companions (Becker et al. 2015) to hot Jupiters? What are the connections between hot Jupiters and warm Jupiters (Huang et al. 2016), hot Neptunes (Dong et al. 2018), compact multiple-planet systems (Lee & Chiang 2016), and ultra-short-period planets (Winn et al. 2018)? Answers to these questions may come more easily if we enlarge the sample of hot Jupiters around very bright stars, subject to a wide range of irradiation levels.

The recently commissioned *Transiting Exoplanet Survey Satellite* (*TESS*; Ricker et al. 2015) mission has the main goal of discovering transiting exoplanets around bright and nearby stars, thereby facilitating follow-up studies. A few dozen hot Jupiters orbiting bright ($V \lesssim 10$ mag) stars are expected to emerge from the *TESS* mission (Sullivan et al. 2015; Barclay et al. 2018; Huang et al. 2018). They will always be among the most observationally favorable transiting planets, and as such, they will observed and re-observed in perpetuity as astronomical capabilities advance.

Here we report the first confirmation of a hot Jupiter discovered by the *TESS* mission, HD 202772A b. Sec. 2 presents the data. Sec. 3 describes the derivation of the host star characteristics, and Sec. 4 presents the system parameters based on fitting the available photometry and RV data. Sec. 5 summarizes the results and places this discovery into context.

2. OBSERVATION AND DATA REDUCTION

2.1. *TESS Photometry*

HD 202772 (TIC 290131778, TOI 123) was observed by Camera 1 of the *TESS* spacecraft during the first sector of science operations, between 2018 July 25 and 2018 August 22 (BJD 2458325 to 2458353). The available data have two-minute time sampling ("short cadence"). Some basic parameters of the target are given in Table 1. Given its position in the sky, HD 202772 will not be re-observed during the *TESS* primary mission. The photometric data were analyzed by the Science Processing Operations Center (SPOC) pipeline, based on the NASA *Kepler* mission pipeline (Jenkins et al., *in prep*). The light curve of HD 202772 presented in Fig. 1 shows a clear transit signal. It was listed among the *TESS* Alerts published online on 2018 September 5, prompting us to download the photometric time series.[1]

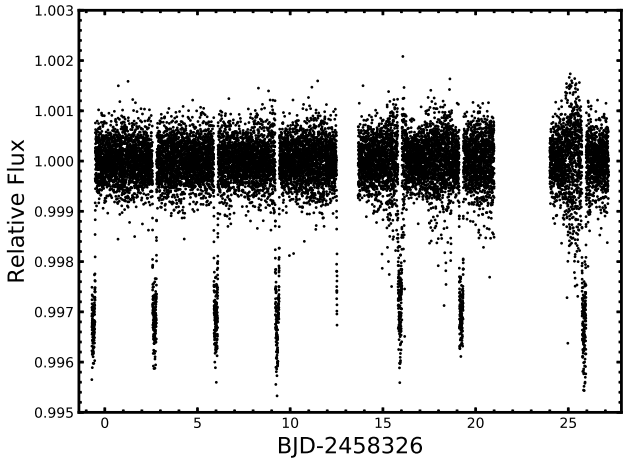

Figure 1. The *TESS* Sector 1 light curve of HD 202772A, with two minute cadence. Instrumental signals have already been removed from these data. The periodic decreases in flux are the transits of HD 202772A b. The gap in the middle of the light curve is due to the data download, which was performed at the end of the satellite's ninth orbit.

We detrended the raw light curves in the following way (see e.g. Günther et al. 2017, 2018). After masking out all of the data obtained during transits, we fitted a Gaussian Process (GP) model to the data, using a Matern 3/2 kernel and a white noise kernel. For this task we employed the CELERITE package, which uses a Taylor-series expansion of these kernel functions. Once the parameters of the GP were constrained based on the out-of-transit data, we used it to detrend the entire light curve.

The SPOC pipeline produces flags for poor-quality exposures. These include exposures taken during the 30-minute long momentum dumps that occurred every 2.5 days (10 times in total). All flagged exposures were

[1] The *TESS* Alerts are currently in a beta test phase. The full set of raw and calibrated data products from *TESS* Sectors 1 through 4, including this source, will be available via NASA's Mikulski Archive for Space Telescopes (MAST) no later than January 2019.

Table 1. HD 202772

Parameter	HD 202772A	HD 202772B	Source
R.A. (hh:mm:ss)	21:18:47.901	21:18:47.813	Gaia DR2
Dec. (dd:mm:ss)	−26:36:58.95	−26:36:58.42	Gaia DR2
μ_α (mas yr^{-1})	28.360 ± 0.269	23.236 ± 0.157	Gaia DR2
μ_δ (mas yr^{-1})	−56.533 ± 0.418	−57.557 ± 0.152	Gaia DR2
Parallax (mas)	6.166 ± 0.092	6.686 ± 0.109	Gaia DR2
B (mag)	8.81 ± 0.02	10.65 ± 0.02	Tycho
V (mag)	8.320 ± 0.05	10.15 ± 0.05	Tycho
TESS (mag)	7.92 ± 0.09	9.62 ± 0.09	TIC V7[1]
J (mag)	7.437 ± 0.027	9.142 ± 0.029	NIRC2; this paper
H (mag)	7.266 ± 0.021	8.897 ± 0.022	NIRC2; this paper
Ks (mag)	7.149 ± 0.017	8.858 ± 0.018	NIRC2; this paper
Spectroscopic and Derived Properties			
$T_{\rm eff}$ (K)	6330 ± 100	6156 ± 100	Keck/HIRES; this paper
$\log g_*$ (cgs)	4.03 ± 0.10	4.24 ± 0.10	Keck/HIRES; this paper
[Fe/H] (dex)	0.29 ± 0.06	0.25 ± 0.06	Keck/HIRES; this paper
M_* ($M_\odot$)	$1.69^{+0.05}_{-0.04}$	1.21 ± 0.04	Keck/HIRES; this paper
R_* ($R_\odot$)	$2.515^{+0.137}_{-0.127}$	1.16 ± 0.06	Keck/HIRES; this paper
Age (age)	$1.52^{+0.19}_{-0.20}$	$1.27^{+1.32}_{-0.80}$	Keck/HIRES; this paper

[1] Stassun et al. (2018)

Table 2. HD 202772A

Parameter	SMARTS 1.5m/CHIRON	FLWO 1.5m/TRES	LCO/NRES	KECK/HIRES	EXOFASTv2 FIT
$T_{\rm eff}$ [K]	6470 ± 100	6270 ± 50	6255 ± 100	6330 ± 100	6230^{+110}_{-98}
$\log g_*$ [cgs]	3.90 ± 0.15	3.91 ± 0.10	4.0 ± 0.1	4.03 ± 0.10	3.835 ± 0.034
[Fe/H] [dex]	0.30 ± 0.10	0.16 ± 0.08	0.27 ± 0.06	0.29 ± 0.06	$0.29^{+0.13}_{-0.24}$
M_* [$M_\odot$]	1.73 ± 0.05	...	$1.78^{+0.02}_{-0.06}$	$1.69^{+0.05}_{-0.04}$	$1.703^{+0.075}_{-0.12}$
R_* [$R_\odot$]	2.65 ± 0.15	...	$2.87^{+0.11}_{-0.10}$	$2.515^{+0.137}_{-0.127}$	$2.614^{+0.08}_{-0.11}$
Age [Gyr]	1.6 ± 0.1	...	$1.48^{+0.24}_{-0.16}$	$1.52^{+0.19}_{-0.20}$	$1.80^{+0.43}_{-0.30}$
$V \sin i$ [km s^{-1}]	...	8.1 ± 0.5	5.5 ± 1.4	7.0 ± 1.0	...

omitted from our analysis. The resulting light curve is plotted in Fig. 1.

2.2. *Keck/NIRC2 Adaptive Optics Imaging*

HD 202772 was reported to be a pair of stars in several wide-field surveys (e.g. Tycho-2, Høg et al. 2000; PPMXL, Roeser et al. 2010; Gaia DR2, Gaia Collaboration et al. 2018; see also Holden 1978, Horch et al. 2001) reported two bright stars separated by ≈1.5″, although the *Gaia* DR 2 catalog flags the brighter star as a "duplicate" entry. To check on these earlier findings, we performed high-resolution adaptive optics (AO) imaging at Keck Observatory.

The Keck observations were made with the NIRC2 instrument on Keck-II behind the natural guide star AO system. The observations were made on 2018 September 18 on a night with partial cirrus conditions. We used the standard 3-point dither pattern that avoids the left lower quadrant of the detector (which is typically noisier than the other three quadrants). The dither pattern step size was 3″, and it was repeated twice, with the second dither offset from the first dither by 0.5″. Observations were made with three different filters: narrow-band Br_γ ($\lambda_o = 2.1686; \Delta\lambda = 0.0326\,\mu$m), H-continuum ($\lambda_o = 1.5804; \Delta\lambda = 0.0232\,\mu$m), and J-continuum ($\lambda_o = 1.2132; \Delta\lambda = 0.0198\,\mu$m), using inte-

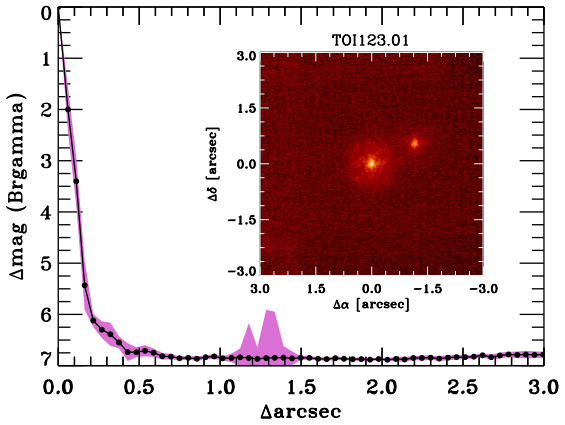

Figure 2. AO image (inset) and K_s-band contrast curves for HD 202772A, obtained with Keck/NIRC2. A companion is visible 1.3″ northwest of the primary. The black line is the 5σ sensitivity, with a 1σ scatter marked in purple. See text for further details.

gration times of 1.45, 5.0, and 1.5 seconds, respectively. The camera was in the narrow-angle mode with a full field of view of 10″ and a pixel scale of approximately 0.01″ per pixel.

Two stars were clearly detected, with a separation of 1.3″ (Figure 2). The resolution of the 2 μm image is approximately 0.05″ FWHM. The sensitivity of the final combined AO image was determined by injecting simulated sources azimuthally around the primary target every 45° at separations of integer multiples of the FWHM of the central source (Furlan et al. 2017). The brightness of each injected source was scaled until standard aperture photometry detected it with 5σ significance. The resulting brightness of the injected sources relative to our target was taken to be the contrast limit for the injected location. The final 5σ limit at each separation was determined from the average of all of the determined limits at that separation, with an uncertainty given by the RMS dispersion of the results for different azimuthal slices. Figure 2 shows the 2 μm sensitivity curve in black, with the 1σ (RMS) dispersion marked in purple. The inset image shows the primary target in the center and the second source located 1.3″ to the northwest.

The two stars were detected in all three filters. The presence of the blended companion must be taken into account to obtain the correct transit depth and planetary radius (Ciardi et al. 2015). The stars have blended 2MASS magnitudes of $J = 7.232 \pm 0.026$ mag, $H = 7.048 \pm 0.021$ mag, and $K_s = 6.945 \pm 0.026$ mag. The stars have measured magnitude differences of $\Delta J = 1.705 \pm 0.0015$ mag, $\Delta H = 1.631 \pm 0.008$ mag, and $\Delta K_s = 1.709 \pm 0.011$ mag. The primary star has deblended apparent magnitudes of $J_1 = 7.437 \pm 0.027$ mag, $H_1 = 7.266 \pm 0.021$ mag, and $Ks_1 = 7.149 \pm 0.017$ mag, corresponding to $(J - H)_1 = 0.171 \pm 0.034$ mag and $(H - K_s)_1 = 0.117 \pm 0.027$ mag. The secondary star has deblended apparent magnitudes of $J_2 = 9.142 \pm 0.029$ mag, $H_2 = 8.897 \pm 0.022$ mag, and $Ks_2 = 8.858 \pm 0.018$ mag, corresponding to $(J-H)_2 = 0.245 \pm 0.036$ mag and $(H - K_s)_2 = 0.039 \pm 0.029$ mag. The infrared colors of the primary star are consistent with an early-G or late-F main sequence star, in agreement with the derived stellar parameters. The companion star has infrared colors that are consistent with a later G-type main sequence star.

Based on the *TESS* magnitude and 2MASS color relationships established for the *TESS* Input Catalog (Stassun et al. 2018), we estimate that the deblended *TESS* magnitudes for the two components to be $T_1 = 7.92 \pm 0.09$ mag and $T_2 = 9.62 \pm 0.09$ mag for a *TESS* magnitude difference of $\Delta_T = 1.7 \pm 0.1$ mag and a *TESS* flux ratio of $F_2/F_1 = 0.21 \pm 0.02$. We used this value of the flux ratio to correct the apparent transit depth in the *TESS* light curve, and derive the unblended transit depth.

We will refer to the brighter target (hosting the planet) as HD 202772A, and the fainter companion as HD 202772B. Given the similarity between the two stars, and a projected separation of only ~ 200 AU, it seems very likely that the two stars are gravitationally bound. The chance alignment probability is negligible, as estimated from the Besançon Galactic Model (Robin et al. 2003). We have also checked all 131 stars in the Gaia DR2 catalog within 300 ″ of HD 202772A with measured parallax and proper motion, and the only nearby source with a similar projected velocity is HD 202772B.

2.3. *LCO/NRES Optical Spectroscopy*

To obtain independent estimates of the stellar parameters, we performed high-resolution optical spectroscopy with the Las Cumbres Observatory (LCO) robotic network of telescopes (Brown et al. 2013). We obtained three 20-minute exposures with a total signal-to-noise ratio (SNR) ≈100 with the Network of Echelle Spectrographs (NRES; Siverd et al. 2016, 2018) mounted on a 1.0m telescope at the South African Astronomical Observatory (SAAO).

Since the NRES fiber diameter corresponds to 2.8″, it captured the light from both stars in the visual binary system. Using TODCOR (Zucker & Mazeh 1994), we identified two RV components separated by 5 ± 1 km s^{-1}. This RV difference is compatible with the order of magnitude of the RV variation one would expect from the

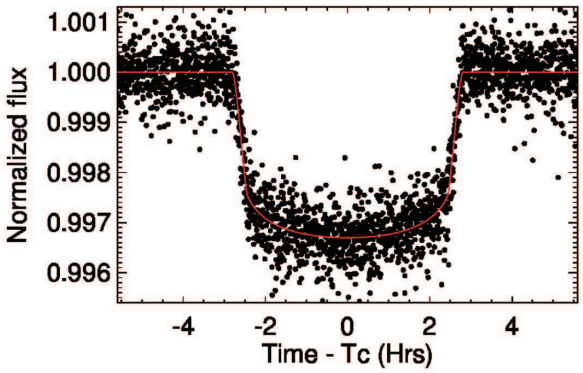

Figure 3. Phased light curves of HD 202772A b. The red solid line represents the best-fitting model.

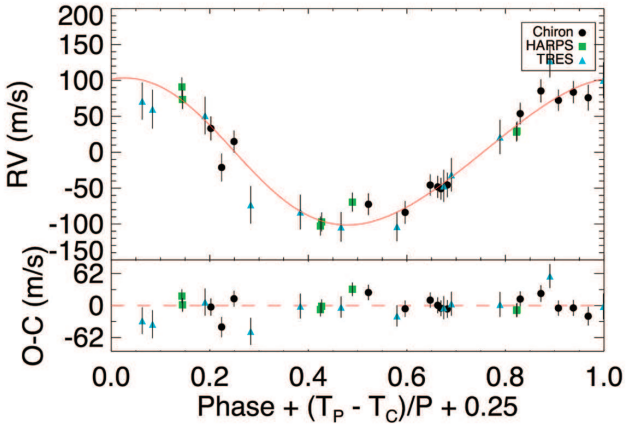

Figure 4. RV measurements from CHIRON (black circles), HARPS (green squares), and TRES (blue triangles) as a function of orbital phase. The error bars include the fitted jitter term. The units of the horizontal axis are chosen so the time of transit is at 0.25. The solid red line is the best-fitting model, based on the transit photometry as well as the RV data. The fitted value of the systemic velocity has been subtracted from both the RVs and the model. The bottom panel presents the residuals between the data and the best fit model.

orbital motion of the stars, given their masses and sky-projected separation.

2.4. *Keck/HIRES Optical Spectroscopy*

In order to obtain a spectrum of each of the two stars with minimal contamination from the other star, we observed both stars with Keck/HIRES (Vogt et al. 1994) on 2018 September 23. We obtained one spectrum of each star, with the HIRES slit oriented perpendicular to the separation between the two stars. Given the angular separation between the two stars, the slit width (0.86″) and the astronomical seeing at Keck at the night of the observation (≈0.7″), the level of cross-contamination is expected to be less than 10%. Both spectra were obtained without the iodine (I_2) cell, at a spectroscopic resolution of R≈65,000, and at a signal-to-noise ratio per pixel of 150 at 5500 Å. A similar technique was successfully applied by Shporer et al. (2014) to a visual binary system in which both members have similar brightness and a smaller angular separation.

2.5. *Doppler Velocimetry with CHIRON*

We obtained a total of 14 spectra of HD 202772A using CHIRON (Tokovinin et al. 2013), a fiber-fed high-resolution optical spectrograph mounted on the SMARTS 1.5m telescope at Cerro Tololo in Chile. We collected the spectra using the image slicer, which delivers a resolution of ∼80,000 and a higher throughput than the standard slit mode. Our 15-minute exposures yielded a SNR per pixel of ∼60-80 at 5500 Å.

Although CHIRON is equipped with an iodine cell to obtain a precise wavelength solution that permits long-term RV precision better than ∼ 2-3 $\mathrm{m\,s^{-1}}$ (e.g. Jones et al. 2017), we did not use the iodine cell for these observations. This is because the cell absorbs ∼ 25 % of the light at 5500Å, significantly decreasing the signal-to-noise ratio. Moreover, using the I_2 cell requires a time-consuming acquisition of a high-SNR template spectrum of the target star.

Instead, we derived the RVs using the Cross-Correlation-Function (CCF) method, in a manner similar to Jones et al. (2017). CHIRON is not equipped with a simultaneous calibration fiber. Instead, we acquired a Th-Ar lamp exposure before and after each target exposure. We computed the wavelength solution for the target spectra by interpolating line positions for the lamps to match the temporal midpoint of each observation. We thereby achieved a RV stability of ∼ 5-6 $\mathrm{m\,s^{-1}}$, which was verified with two RV standard stars observed nightly. The resulting RVs of HD 202772A are listed in Table 3. RVs collected by CHIRON show a ∼ 95 $\mathrm{m\,s^{-1}}$ sinusoidal variation in phase with the transit ephemeris.

Finally, from the CCF, we measured the bisector velocity span (BVS) and FWHM variations, to check on the possibility that the observed RV variation results from stellar activity or a background eclipsing binary system (see, e.g., Santerne et al. 2015). Fig. 6 shows the BVS and FWHM as a function of the measured radial velocities. There is no significant correlation between these quantities and the radial velocities.

The CHIRON fiber has a 2.7″ diameter on the sky, but HD 202772A and B are separated by only 1.3″, which means that we must expect some of the light from the

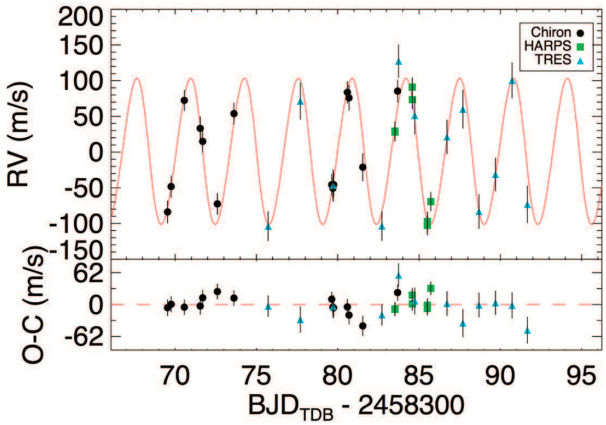

Figure 5. Same as Figure 4, but as a function of time instead of orbital phase.

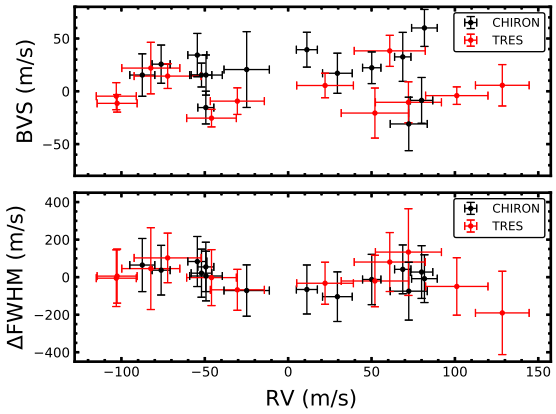

Figure 6. Bisector velocity span (BVS; top panel) and CCF FWHM (bottom panel) as functions of the radial velocities collected by SMARTS 1.5m/CHIRON and FLWO 1.5m/TRES.

binary companion to be present in the spectra. Given that the two stars have a similar radial velocity, there is a risk that the stationary CCF of the binary companion causes the apparent amplitude of the RV variation to be lower than the true RV variation of the planet host. Such a "peak pulling" effect was observed in a study of the Kepler-14 system (Buchhave et al. 2011). We note, however, that HD 202772B is fainter than HD 202772A and only emits about 20% of the total light from the binary system. As described in Section 2.7, we did not find any evidence that the RVs from CHIRON were significantly affected by light contamination from HD 202772B.

2.6. *Doppler Velocimetry with FLWO 1.5m/TRES*

We obtained 12 spectra of HD 202772A with the Tillinghast Reflector Echelle Spectrograph (TRES; Fűrész 2008) on the 1.5m Tillinghast Reflector at Fred L. Whipple Observatory (FLWO) on Mt. Hopkins, AZ between UT 2018 September 14 and UT 2018 September 30. TRES is a fiber-fed, cross-dispersed echelle spectrograph with a resolving power of $R \sim 44,000$ and an instrumental precision of $\sim$ 10–15 m s^{-1}. The typical exposure time was $\sim$ 4 minutes, resulting in SNR per resolution element of $\sim$ 75 at 5200 Å. The spectra are calibrated using a ThAr lamp, exposed through the science fiber before and after each set of science exposures. We note that the TRES fiber is 2.3″, and the exposures therefore include light from HD 202772B.

We reduced and analyzed the spectra according to the procedures outlined in Buchhave et al. (2010). Namely, the spectra were optimally extracted and then cross-correlated, order by order, against the strongest spectrum of HD 202772A. We exclude spectral orders far to the blue where the SNR is low, in the red where telluric lines contaminate the spectrum, and a few orders in between with little information content or affected by broad feature (e.g., Balmer lines) toward the edge of the order that affect continuum fitting. RVs were ultimately derived from a region spanning 4130–6280 Å. The peak of the summed CCF across all orders is fit to derive the final RV, and the scatter between orders within a each spectrum is taken to be the internal error estimate. These relative RVs and their uncertainties are reported in Table 3.

We also derive the BVS and FWHM from the cross-correlation function of each spectrum against a non-rotating synthetic spectrum with appropriate $T_{\rm eff}$, $\log g_*$, and [Fe/H]. These values are also reported in Table 3 and shown in Figure 6, and show no correlation with the RVs.

2.7. *Doppler Velocimetry with HARPS*

To provide further confirmation of the planetary origin of the transit signal, we obtained 9 spectra using the High Accuracy Radial velocity Planet Searcher (HARPS; Mayor et al. 2003). These data were obtained during three consecutive nights in good seeing conditions ($\lesssim$ 1.0″). Exposure time was 200-300 seconds, leading to a SNR of $\sim$ 70-80 at 6,000 Å. We carefully centered the brighter star within the 1″ aperture fiber, to ensure that no light contamination from the companion was reaching the detector. We also carefully adjusted the size of the guiding box, to avoid guiding problems due to the secondary star, which was clearly visible in the acquisition camera. During the HARPS observations, the Moon was between 13° and 36° from our target, with an illuminated fraction between 92% and 99%. This led to some lunar contamination in the spectra. Moreover,

the RV of the Moon was very close to the RV of the target star, which severely affected the shape of the CCF. For this reason, we discarded the two RV data points that were most affected and had very deviant values. Also, due to the contamination, the derived BVS and FWHM of the CCF are not reliable, and are not listed in Table 3. We processed the HARPS data using the CERES code (Brahm et al. 2017). The resulting RVs are listed in Table 3, and also shown in Figure 4. As can be seen, the HARPS data agree with the CHIRON data, although the scatter around the fit is larger than expected. This is most likely caused by the lunar light contamination.

3. STELLAR PARAMETERS

3.1. *Results from CHIRON*

To derive the stellar atmospheric parameters of HD 202772A we measured the equivalent widths (EWs) of about 150 relatively weak Fe I and Fe II absorption lines (EW $\lesssim 120$ mÅ). The EWs were measured in the high-SNR template obtained by stacking the individual spectra (see Sec. 2.5), using the ARES v2 automatic tool (Sousa et al. 2015).

We then used the MOOG code (Sneden 1973) along with the Kurucz (1993) stellar atmosphere models to solve the radiative transfer equations under the assumptions of local excitation and ionization equilibrium via the Saha and Boltzmann equations. For each iron line, MOOG computes the corresponding iron abundance by matching the measured EW in the curve of growth computed from the input stellar model. This procedure is performed iteratively for models with different effective temperatures ($T_{\rm eff}$), iron abundances ([Fe/H]), and micro-turbulent velocities ($V_{\rm micro}$) until there is no correlation between the line excitation potential and wavelength with the model abundance. Finally, we obtained the surface gravity ($\log g_*$) using the constraint that the iron abundances derived from both the Fe I and Fe II lines should be the same (For a more thorough description of the procedure, see Jones et al. 2011). Table 2 gives the resulting stellar parameters.

We computed the luminosity of HD 202772A based on the Gaia DR2 parallax ($\pi = 6.166 \pm 0.092$, Gaia Collaboration et al. 2018), the apparent V magnitude (after correcting for interstellar absorption by $A_V = 0.10$ mag), and the bolometric correction of (Alonso et al. 1999). Using this information and the stellar atmospheric parameters ($T_{\rm eff}$ and [Fe/H]), we derived the stellar physical parameters using the PARSEC stellar-evolutionary models (Bressan et al. 2012). The results are also listed in Table 2.

3.2. *Results from FLWO 1.5m/TRES*

We used the Spectral Parameter Classification (SPC) tool (Buchhave et al. 2012) to derive stellar parameters from the TRES spectra. We allowed $T_{\rm eff}$, $\log g_*$, [Fe/H], and $V \sin i$ to be free parameters. SPC works by cross correlating an observed spectrum against a grid of synthetic spectra based on Kurucz atmospheric models (Kurucz 1993). The weighted average results are listed in Table 2.

3.3. *Results from LCO/NRES*

We analyzed the LCO/NRES spectrum using the methodology of Fulton & Petigura (2018). We measured $T_{\rm eff}$, $\log g_*$, [Fe/H], and $V \sin i$ using `SpecMatch` (Petigura 2015)[2], which compares the observed spectrum with a grid of model spectra (Coelho et al. 2005). The resulting parameters are listed in Table 2.

To calculate the star's physical parameters, we used `isoclassify` (Huber et al. 2017), which takes as input the effective temperature, metallicity, parallax, and apparent K_s magnitude. Using the `isoclassify` "direct" mode, we calculated the posterior probability distributions for $R_\star$ and $L_\star$ by applying the Stefan–Boltzmann law. Using the `isoclassify` "grid" mode, we calculated the range of MIST isochrone models (Dotter 2016; Choi et al. 2016) that are consistent with the spectroscopic parameters to estimate the stellar mass and age. The results of the `SpecMatch`+`isoclassify` analysis are listed in Table 2.

3.4. *Results from Keck/HIRES*

The Keck/HIRES spectrum of each of the two stars was also analyzed using `SpecMatch`. The resulting atmospheric and physical stellar parameters for both HD 202772A and B are listed in Table 1 and Table 2.

The stellar parameters derived from resolved HIRES spectra show good agreement with those from the CHIRON, TRES, and NRES spectra, except that TRES finds modestly lower [Fe/H]. Evidently, the contaminating light from the secondary star in the CHIRON, TRES, and NRES spectra did not strongly affect the determination of the basic stellar parameters.

4. PLANETARY SYSTEM PARAMETERS FROM GLOBAL ANALYSIS

We performed a joint analysis of the *TESS* data, the RV data, and the stellar spectral energy distribution using EXOFASTv2[3] (Eastman et al. 2013, 2017).

[2] https://github.com/petigura/specmatch-syn
[3] https://github.com/jdeast/EXOFASTv2

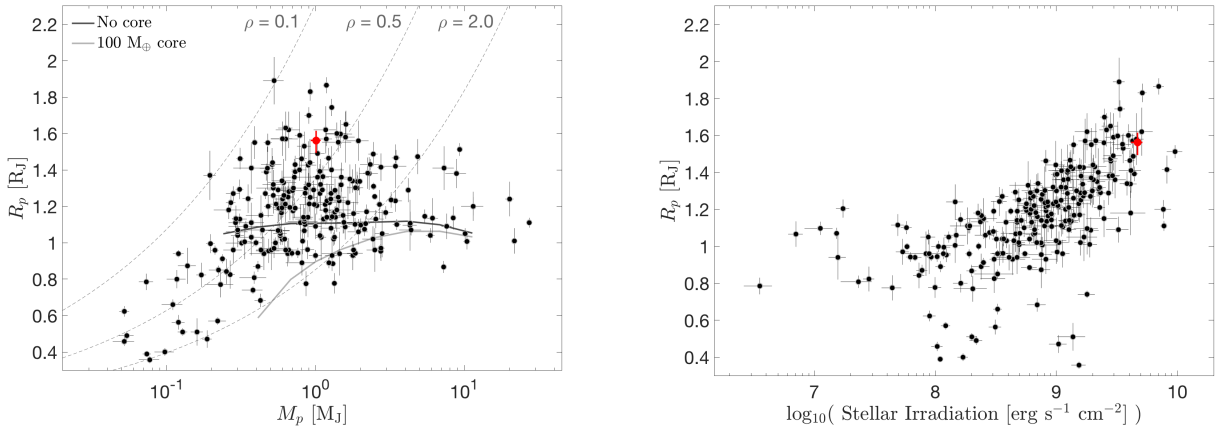

Figure 7. The position of HD 202772A b (red) in the space of mass, radius, and irradiation, compared to the population of known transiting gas giant planets (black). In the left panel, the solid lines mark theoretical models taken from Baraffe et al. (2014) for no core (black) and a 100 M_{Earth} core (gray). The dashed lines are isodensity contours. Data were obtained from the NASA Exoplanet Archive (Akeson et al. 2013) on 2018 September 15.

The stellar limb darkening function was assumed to be quadratic, with the coefficients fit with a prior from Claret (2018) for the *TESS* band based on the $\log g_*$, $T_{\rm eff}$, and [Fe/H] at each step. We imposed Gaussian priors on the Gaia DR2 parallax of 6.77 ± 0.11 mas (after adjusting by 82 μas as advocated by Stassun et al. 2018) and the *TESS*-band dilution from the neighboring star of 0.21 ± 0.02 found from the AO imaging. We imposed an upper limit on the V-band extinction of 0.17236 from Schlafly & Finkbeiner (2011). The priors for all the remaining parameters were uniform and unbounded.

To constrain the spectral energy distribution, we use the broadband photometry from Tycho (which resolved the companion), and the 2MASS JHK photometry after deblending based on the Keck AO images. We opted not to impose any informative priors on the spectroscopic parameters $T_{\rm eff}$ or [Fe/H]. Instead, we relied on the observed spectral energy distribution and the MIST stellar-evolutionary models to constrain the stellar parameters. The resulting stellar parameters are listed in Table 2, and show good agreement with the results of the spectroscopic analysis. Table 4 gives the results of the EXOFAST fit to all of the data. The best-fitting model is also plotted in Figures 3, 4, and 5.

5. DISCUSSION

HD 202772A b is an inflated Jupiter-mass planet orbiting a metal-rich star with an orbital period of 3.3 days. The red dots in Fig. 7 show the location of this newly discovered planet in the spaces of planetary mass, radius, and incident flux, compared with the current sample of transiting giant planets. HD 202772A b is one of the largest known planets, with a relatively low mean density of 0.33 g cm^{-3}. It is also one of the most strongly irradiated planets, thereby obeying the well known correlation between planetary radius and degree of irradiation (see, e.g., Laughlin et al. 2011; Lopez & Fortney 2016). Based on the irradiation of 4.7×10^9 erg s^{-1} cm^{-2}, the estimated equilibrium temperature is about 2,100 K (see Table 4).

The large size of HD 202772A b might be connected to the evolutionary state of the host star (Grunblatt et al. 2017). Fig. 8 shows the location of HD 202772A in the space of surface gravity and effective temperature. HD 202772A is slightly evolved, with a relatively low surface gravity. As a star evolves, its luminosity increases, which also increases the flux of radiation impinging on any planets. If giant planets are "inflated" by intense stellar radiation, as has long been proposed, then the larger-than-usual size of HD 202772A b suggests that the evolutionary timescale of the star is slower than the inflationary timescale of the planet.

HD 202772A will exhaust its hydrogen fuel in $\sim$ 0.5 Gyrs, which may have ramifications for the survival of the planet. The apparent paucity of hot Jupiters orbiting evolved stars (Johnson et al. 2007) has been interpreted as a consequence of tidal destruction (Villaver & Livio 2009; Schlaufman & Winn 2013). Tides raised on the star by the planet cause the planet to transfer angular momentum to the star, a process that is thought to accelerate rapidly as the star grows in size. However, the timescale for this process is unknown, with an uncertainty spanning several orders of magnitude.

The recent discoveries of close-in gas giants around subgiants (e.g. Van Eylen et al. 2016), or even red giants (e.g. Jones et al. 2018) suggest that the lifetimes of hot Jupiters in those systems may not as short as we

Table 3. Relative radial velocities for HD 202772A

BJD	RV	σ_{RV}	BVS[1]	σ_{BVS}	FWHM[1]	σ_{FWHM}	Instrument
-2458300	m s^{-1}	m s^{-1}	m s^{-1}	m s^{-1}	m s^{-1}	m s^{-1}	
69.5363	-87.5	7.5	15.4	20.1	16302.0	141.5	CHIRON
69.7550	-52.0	6.2	15.4	11.3	16258.7	128.1	CHIRON
70.5656	68.7	4.9	32.6	23.2	16279.1	130.0	CHIRON
71.5411	29.5	8.9	17.1	19.0	16133.5	132.2	CHIRON
71.6964	11.2	6.3	39.4	16.5	16171.8	130.5	CHIRON
72.5988	-76.2	5.4	25.7	18.1	16274.6	132.2	CHIRON
73.6179	50.1	5.5	22.3	15.0	16225.0	133.9	CHIRON
79.6314	-49.4	4.8	-15.4	15.5	16292.1	131.5	CHIRON
79.7038	-54.5	5.7	34.3	20.5	16320.8	133.3	CHIRON
79.7466	-49.3	9.8	15.4	19.0	16243.6	132.4	CHIRON
80.5925	80.0	6.7	-8.6	21.7	16264.7	140.5	CHIRON
80.6924	72.3	11.1	-30.9	25.3	16162.8	154.1	CHIRON
81.5400	-24.9	13.6	20.6	35.9	16166.2	136.7	CHIRON
83.6838	81.7	7.7	60.0	17.5	16229.4	127.2	CHIRON
83.5215	34.8	2.0	...	...	...	...	HARPS
83.5252	36.3	2.0	...	...	...	...	HARPS
84.5863	80.3	2.0	...	...	...	...	HARPS
84.5837	97.8	2.4	...	...	...	...	HARPS
85.5194	-90.3	2.8	...	...	...	...	HARPS
85.5128	-96.0	2.8	...	...	...	...	HARPS
85.7274	-62.7	2.0	...	...	...	...	HARPS
75.7239	-0.5	12.0	-4.6	12.8	18858	151	TRES
77.6977	174.7	19.8	-10.4	19.4	18997	231	TRES
79.7226	56.6	14.9	-25.4	8.3	18861	149	TRES
82.7170	0.0	12.0	-11.4	8.3	18869	144	TRES
83.7441	231.0	16.1	5.7	19.6	18673	222	TRES
84.7374	154.6	20.2	-20.6	23.7	18843	137	TRES
86.7178	124.7	17.0	5.5	11.6	18831	112	TRES
87.6938	163.5	21.3	38.3	14.7	18944	157	TRES
88.6862	20.2	17.4	22.0	24.4	18909	218	TRES
89.7004	72.1	16.2	-9.3	12.6	18796	109	TRES
90.7214	203.7	18.7	-4.1	8.3	18814	153	TRES
91.6617	30.3	20.1	14.4	11.7	18966	132	TRES

[1] The HARPS BVS and FWHM are not listed because those measurements were corrupted by moonlight (Section 2.7).

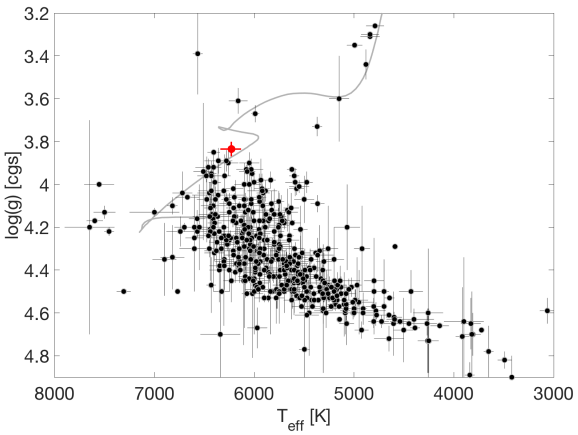

Figure 8. Surface gravity and effective temperature of the hosts of transiting giant planets (similar to an H-R diagram). The position of HD 202772A (red) falls near the edge of the occupied region of parameter space. The solid gray line is the best-fitting MIST stellar mass track. Data were obtained from the NASA Exoplanet Archive (Akeson et al. 2013) on 2018 September 15.

thought. Alternatively, as predicted by Stephan et al. (2018), the eccentric Kozai-Lidov mechanism in a binary stellar system can drive a longer period Jupiter migrate inward during the post-main sequence phase. It seems that with the distant stellar companion, HD 202772A b is consistent with this scenario. A likely prediction from this scenario is that HD 202772A b may have a non zero stellar obliquity (the angle between the orbital axis and the stellar spin axis), which can be tested in future observations. From the stellar and planetary parameters we obtained, we predict that the Rossiter-Mclaughlin effect with have an RV semiamplitude of 10.5 m s^{-1} (e.g., Winn et al. 2005; Gaudi & Winn 2007; Albrecht et al. 2012; Wang et al. 2018).

However, it is impossible to draw any firm conclusions until we can measure the occurrence rates of such planets using a homogenoeous data set. The *TESS* survey should eventually provide the opportunity to perform such a study, by detecting thousands of new planets orbiting a wider variety of stars than were observed in the *Kepler* mission.

We thank Yanqin Wu, Smadar Naoz, Lars A. Buchhave, Bonan Pu, Alexander P. Stephan, Sabarni Basu, Beibei Liu, and Jorge Lillo-Box for their insights. J.N.W. and S.W. thanks the Heising-Simons Foundation for their generous support. M.N.G. acknowledges support from MIT's Kavli Institute as a Torres postdoctoral fellow. S.M. and A.B.D. are supported by the National Science Foundation Graduate Research Fellowship Program under Grant Number DGE-1122492. R.B. acknowledges support from FONDECYT Postdoctoral Fellowship Project 3180246, and from the Millennium Institute of Astrophysics (MAS). This research is based on observations collected at the European Organization for Astronomical Research in the Southern Hemisphere under ESO programme 0101.C-0232. This work makes use of observations from SMARTS and the LCO network. We acknowledge the use of *TESS* Alert data, which is currently in a beta test phase, from the *TESS* Science Office and the *TESS* Science Processing Operations Center. Funding for the *TESS*

mission is provided by NASA's Science Mission directorate. The authors wish to recognize and acknowledge the very significant cultural role and reverence that the summit of Maunakea has always had within the indigenous Hawaiian community. We are most fortunate to have the opportunity to conduct observations from this mountain This research has made use of the Exoplanet Follow-up Observation Program website, which is operated by the California Institute of Technology, under contract with the National Aeronautics and Space Administration under the Exoplanet Exploration Program. We made use of the Python programming language (Rossum et al. 1995) and the open-source Python packages NUMPY (van der Walt et al. 2011), EMCEE (Foreman-Mackey et al. 2013), and CELERITE (Foreman-Mackey et al. 2017).

Facilities:

Facility: *TESS*,

Facility: CTIO:1.5m (CHIRON),

Facility: ESO:3.6m (HARPS),

Facility: Keck II (NIRC2),

Facility: Keck I (HIRES),

Facility: LCO:1.0m (NRES),

Facility: FLWO:1.5m (TRES)

Table 4. Median values and 68% confidence interval for HD 202772A planetary system.

Parameter	Units	Values
Stellar Parameters:		
M_*	Mass ($M_\odot$)	$1.703^{+0.075}_{-0.12}$
R_*	Radius ($R_\odot$)	$2.614^{+0.080}_{-0.11}$
L_*	Luminosity ($L_\odot$)	$9.25^{+0.58}_{-0.60}$
ρ_*	Density (cgs)	$0.134^{+0.017}_{-0.014}$
$\log g_*$	Surface gravity (cgs)	3.835 ± 0.034
$T_{\rm eff}$	Effective Temperature (K)	6230^{+110}_{-98}
[Fe/H]	Metallicity (dex)	$0.29^{+0.13}_{-0.24}$
Age	Age (Gyr)	$1.80^{+0.43}_{-0.30}$
A_V	V-band extinction (mag)	$0.101^{+0.050}_{-0.062}$
σ_{SED}	SED photometry error scaling	$3.6^{+3.8}_{-1.5}$
ϖ	Parallax (mas)	6.79 ± 0.11
d	Distance (pc)	$147.2^{+2.5}_{-2.4}$
Planetary Parameters:		b
P	Period (days)	3.308960 ± 0.000082
R_P	Radius (R_J)	$1.562^{+0.053}_{-0.069}$
T_C	Time of conjunction ($\rm BJD_{TDB}$)	$2458328.68358 \pm 0.00035$
T_0	Optimal conjunction Time ($\rm BJD_{TDB}$)	$2458338.61046 \pm 0.00024$
a	Semi-major axis (AU)	$0.05190^{+0.00075}_{-0.0012}$
i	Inclination (Degrees)	$84.20^{+1.1}_{-0.86}$
e	Eccentricity	$0.047^{+0.050}_{-0.033}$
ω_*	Argument of Periastron (Degrees)	88^{+34}_{-120}
T_{eq}	Equilibrium temperature[1] (K)	2132^{+37}_{-33}
M_P	Mass (M_J)	$1.008^{+0.074}_{-0.079}$
K	RV semi-amplitude (m/s)	$96.9^{+6.1}_{-6.0}$
$logK$	Log of RV semi-amplitude	$1.986^{+0.026}_{-0.028}$
R_P/R_*	Radius of planet in stellar radii	$0.06144^{+0.00083}_{-0.00081}$
a/R_*	Semi-major axis in stellar radii	$4.27^{+0.17}_{-0.15}$
δ	Transit depth (fraction)	$0.003775^{+0.00010}_{-0.000099}$
$Depth$	Flux decrement at mid transit	$0.003775^{+0.00010}_{-0.000099}$
τ	Ingress/egress transit duration (days)	0.0165 ± 0.0011
T_{14}	Total transit duration (days)	$0.2345^{+0.0011}_{-0.0012}$
T_{FWHM}	FWHM transit duration (days)	$0.21797^{+0.00062}_{-0.00058}$
b	Transit Impact parameter	$0.416^{+0.055}_{-0.078}$
ρ_P	Density (cgs)	$0.330^{+0.046}_{-0.036}$
$logg_P$	Surface gravity	$3.012^{+0.041}_{-0.039}$
$\langle F \rangle$	Incident Flux (10^9 erg s^{-1} cm^{-2})	$4.68^{+0.32}_{-0.28}$
T_P	Time of Periastron ($\rm BJD_{TDB}$)	$2458328.74^{+0.49}_{-0.35}$
T_S	Time of eclipse ($\rm BJD_{TDB}$)	$2458330.330^{+0.043}_{-0.051}$
$ecos\omega_*$		$-0.004^{+0.020}_{-0.024}$
$esin\omega_*$		$0.036^{+0.056}_{-0.037}$
$M_P \sin i$	Minimum mass (M_J)	$1.002^{+0.074}_{-0.079}$
M_P/M_*	Mass ratio	$0.000572^{+0.000042}_{-0.000037}$
d/R_*	Separation at mid transit	$4.12^{+0.30}_{-0.36}$

Table 4 continued

Table 4 *(continued)*

Parameter	Units	Values		
Wavelength Parameters:		TESS		
u_1	linear limb-darkening coeff	$0.244^{+0.031}_{-0.032}$		
u_2	quadratic limb-darkening coeff	$0.220^{+0.044}_{-0.042}$		
A_D	Dilution from neighboring stars	0.209 ± 0.020		
Telescope Parameters:		Chiron	HARPS	TRES
$\gamma_{\rm rel}$	Relative RV Offset (m/s)	$-2.9^{+4.7}_{-5.2}$	$9.9^{+9.8}_{-10.}$	$97.8^{+8.5}_{-8.8}$
σ_J	RV Jitter (m/s)	$14.8^{+5.5}_{-4.1}$	$25.6^{+15}_{-8.2}$	$24.5^{+11}_{-8.4}$

[1] Assuming zero albedo and full heat distribution from day to night hemispheres.

REFERENCES

Akeson, R. L., Chen, X., Ciardi, D., et al. 2013, PASP, 125, 989

Albrecht, S., Winn, J. N., Johnson, J. A., et al. 2012, ApJ, 757, 18

Alonso, A., Arribas, S., & Martinez-Roger, C. 1999, A&A, 140, 261

Baraffe, I., Chabrier, G., Fortney, J., & Sotin, C. 2014, Protostars and Planets VI, 763

Barclay, T., Pepper, J., & Quintana, E. V. 2018, arXiv:1804.05050

Batygin, K., Bodenheimer, P. H., & Laughlin, G. P. 2016, ApJ, 829, 114

Becker, J. C., Vanderburg, A., Adams, F. C., Rappaport, S. A., & Schwengeler, H. M. 2015, ApJL, 812, L18

Bodenheimer, P., Hubickyj, O., & Lissauer, J. J. 2000, Icarus, 143, 2

Bonomo, A. S., Desidera, S., Benatti, S., et al. 2017, A&A, 602, A107

Brahm, R., Jordán, A. & Espinoza, N. 2016, PASP, 129, 34002

Bressan, A., Marigo, P., Girardi, L. et al. 2012, MNRAS, 427, 127

Brown, T. M., Baliber, N., Bianco, F. B., et al. 2013, PASP, 125, 1031

Buchhave, L. A., Bakos, G. Á., Hartman, J. D., et al. 2010, ApJ, 720, 118

Buchhave, L. A., Latham, D. W., Carter, J. A., et al. 2011, ApJS, 197, 3

Buchhave, L. A., Latham, D. W., Johansen, A., et al. 2012, Nature, 486, 375

Choi, J., Dotter, A., Conroy, C., et al. 2016, ApJ, 823, 102

Ciardi, D. R., Beichman, C. A., Horch, E. P., & Howell, S. B. 2015, ApJ, 805, 16

Claret, A. 2018, arXiv:1804.10135

Coelho, P., Barbuy, B., Meléndez, J., Schiavon, R. P., & Castilho, B. V. 2005, A&A, 443, 735

Donati, J. F., Moutou, C., Malo, L., et al. 2016, Nature, 534, 662

Dong, S., Xie, J.-W., Zhou, J.-L., Zheng, Z., & Luo, A. 2018, Proceedings of the National Academy of Science, 115, 266

Dotter, A. 2016, ApJS, 222, 8

Duffell, P. C., & Chiang, E. 2015, ApJ, 812, 94

Eastman, J. 2017, Astrophysics Source Code Library, ascl:1710.003

Eastman, J., Gaudi, B. S., & Agol, E. 2013, PASP, 125, 83

Foreman-Mackey, D., Agola, E., Ambikasaran, S., Angus, R. 2017, AJ, 154, 220

Foreman-Mackey, D., Hogg, D. W., Lang, D., Goodman, J. 2013, PASP, 125, 306

Fulton, B. J., & Petigura, E. A. 2018, arXiv:1805.01453

Fűrész, G. 2008, PhD thesis

Furlan, E., Ciardi, D. R., Everett, M. E., et al. 2017, AJ, 153, 71

Gaia Collaboration, Brown, A. G. A., Vallenari, A., et al. 2018, A&A, 616, A1

Gaudi, B. S., & Winn, J. N. 2007, ApJ, 655, 550

Grunblatt, S. K., Huber, D., Gaidos, E., et al. 2017, AJ, 154, 254

Günther, M. N., Queloz, D., Gillen, E., et al. 2017, MNRAS, 472, 295

Günther, M. N., Queloz, D., Gillen, E., et al. 2018, MNRAS, 478, 4720

Høg, E., Fabricius, C., Makarov, V. V., et al. 2000, A&A, 355, L27

Holden, F. 1978, PASP, 90, 587

Horch, E., van Altena, W. F., Girard, T. M., et al. 2001, AJ, 121, 1597
Huang, C. X., Shporer, A., Dragomir, D., et al. 2018, arXiv:1807.11129
Huang, C., Wu, Y., & Triaud, A. H. M. J. 2016, ApJ, 825, 98
Huber, D., Zinn, J., Bojsen-Hansen, M., et al. 2017, ApJ, 844, 102
Johnson, J. A., Fischer, D. A., Marcy, G. W., et al. 2007, ApJ, 665, 785
Jones, M. I., Brahm, R., Espinoza, N., et al. 2018, A&A, 613, A76
Jones, M. I., Brahm, R., Wittenmyer, R. A., et al. 2017, A&A, 602, A58
Jones, M. I., Jenkins, J. S., Rojo, P., & Melo, C. H. F. 2011, A&A, 536, A71
Knutson, H. A., Fulton, B. J., Montet, B. T., et al. 2014, ApJ, 785, 126
Kurucz, R. 1993, ATLAS9 Stellar Atmosphere Programs and 2 km/s grid. Kurucz CD-ROM No. 13. Cambridge, Mass.: Smithsonian Astrophysical Observatory, 1993.
Lai, D. 2016, AJ, 152, 215
Laughlin, G., Crismani, M., & Adams, F. C. 2011, ApJL, 729, L7
Lee, E. J., & Chiang, E. 2016, ApJ, 817, 90
Lin, D. N. C., Bodenheimer, P., & Richardson, D. C. 1996, Nature, 380, 606
Lopez, E. D., & Fortney, J. J. 2016, ApJ, 818, 4
Mayor, M., Pepe, F., Queoz, D., et al. 2003, The Messenger 114, 20
Petigura, E. A. 2015, Ph.D. Thesis,
Petrovich, C. 2015, ApJ, 805, 75
Rasio, F. A., & Ford, E. B. 1996, Science, 274, 954
Ricker, G. R., Winn, J. N., Vanderspek, R., et al. 2015, Journal of Astronomical Telescopes, Instruments, and Systems, 1, 014003
Robin, A. C., Reylé, C., Derrière, S., & Picaud, S. 2003, A&A, 409, 523
Roeser, S., Demleitner, M., & Schilbach, E. 2010, AJ, 139, 2440
Rossum, G. 1995, Python Reference Manual
Santerne, A., Díaz, R. F., Almenare, J.-M. et al, 2015, MNRAS, 451, 2337
Schlafly, E. F., & Finkbeiner, D. P. 2011, ApJ, 737, 103
Schlaufman, K. C., & Winn, J. N. 2013, ApJ, 772, 143
Shporer, A., O'Rourke, J. G., Knutson, H. A., et al. 2014, ApJ, 788, 92
Siverd, R. J., Brown, T. M., Hygelund, J., et al. 2016, Proc. SPIE, 9908, 99086X
Siverd, R. J., Brown, T. M., Stuart, B., et al. 201, Proc. SPIE, 10702, 107026C
Sneden, C. 1973, ApJ, 184, 839
Sousa, S. G., Santos, N. C., Adibekyan, V., Delgado-Mena, E., & Israelian, G. 2015, A&A, 577, A67
Stassun, K. G., Oelkers, R. J., Pepper, J., et al. 2018, AJ, 156, 102
Stephan, A. P., Naoz, S., & Gaudi, B. S. 2018, AJ, 156, 128
Sullivan, P. W., Winn, J. N., Berta-Thompson, Z. K., et al. 2015, ApJ, 809, 77
Tokovinin, A., Fischer, D. A., Bonati, M., et al. 2013, PASP, 125, 1336
van der Walt, S., Colbert, S. C., Varoquaux, G. 2011, Computing in Science & Engineering, 13, 22
Van Eylen, V., Albrecht, S., Gandolfi, D., et al. 2016, AJ, 152, 143
Villaver, E., & Livio, M. 2009, ApJL, 705, L81
Vogt, S. S., Allen, S. L., Bigelow, B. C., et al. 1994, Proc. SPIE, 2198, 362
Wang, S., Addison, B., Fischer, D. A., et al. 2018, AJ, 155, 70
Winn, J. N., Fabrycky, D., Albrecht, S., & Johnson, J. A. 2010, ApJL, 718, L145
Winn, J. N., Noyes, R. W., Holman, M. J., et al. 2005, ApJ, 631, 1215
Winn, J. N., Sanchis-Ojeda, R., & Rappaport, S. 2018, arXiv:1803.03303
Wu, Y., & Lithwick, Y. 2011, ApJ, 735, 109
Wu, Y., Murray, N. W., & Ramsahai, J. M. 2007, ApJ, 670, 820
Zucker, S., & Mazeh, T. 1994, ApJ, 420, 806